Optimum Experimental Design of a Rigid Wing AWE Pumping System

Giovanni Licitra[1], Adrian Bürger[2], Paul Williams[1], Richard Ruiterkamp[1] and Moritz Diehl[3]

***Abstract*— Airborne Wind Energy (AWE) refers to systems capable of harvesting energy from wind by flying crosswind patterns with a tethered aircraft. Accurate models are crucial for tuning and validation of flight controllers. Due to the non-conventional structure of the airborne component, an intensive flight test campaign must be set where maneuvers are performed for parameter estimation purposes. In this paper, we optimize maneuvers for the longitudinal dynamics of a rigid wing AWE pumping system by solving a model-based experimental design problem that aims to obtain more accurate parameter estimates and reduce the flight test time. We consider a trim reference condition of the aircraft and constraints are enforced in order to prevent flight envelope violation. Finally, the optimal solution is implemented in the Flight Control Computer (FCC) of the prototype developed by Ampyx Power B.V. and validated under realistic flight conditions.**

I. INTRODUCTION

Airborne Wind Energy (AWE) is an innovative technology emerging in the renewable energy field. The idea of using tethered aircraft for wind power generation was initially motivated by Loyd [1]. In the last decades, several systems with high power-to-mass ratio and capacity factor have been deployed in order to exploit the wind at high altitude with low costs [2].

Among the different concepts in the landscape of AWE [3][4], one promising case study is the so called AWE *pumping* system. In this technology, the airborne component can be either a soft wing (e.g. kite) or a rigid wing (aircraft) and in both cases the wing exerts a high tension on the tether which is connected to a ground-based generator. A rigid wing AWE pumping system is being developed by Ampyx Power B.V. [5]. Fig. 1 depicts the basic control strategy of the case study while Fig. 2 shows the second generation prototype of the airborne component which is referred to as a *PowerPlane*.

The rigid wing AWE pumping system requires accurate models of the entire system, including the *PowerPlane*. Existing analysis tools such as Computational Fluid Dynamics (CFD) [6] or Lifting-line method [7] are able to provide initial estimates of the parameters, but in most cases the full dynamic effects of the *PowerPlane* have to be determined via an intensive flight test campaign in order to gain additional insight about the aerodynamic properties.

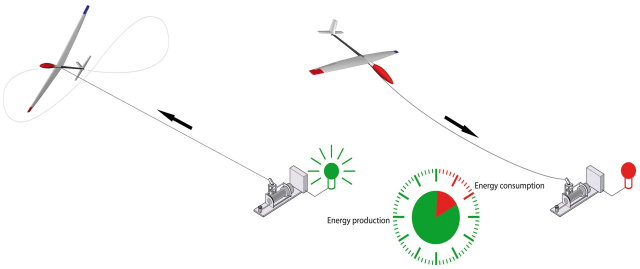

Fig. 1. In a AWE pumping system, a *production phase* follows a *retraction phase* periodically. During the *production phase*, the aircraft exerts a high tension on the tether which is used to rotate a drum that drives an electric generator. In the *retraction phase* the tether is wound up by changing the flight pattern so that significantly less energy needs to be invested in comparison to what has been gained during the *production phase*.

A successful flight test campaign depends on many factors, such as selection of instrumentation, signal conditioning, flight test operations procedure, parameter estimation algorithm and signal input design. In [8] the longitudinal dynamics of the *PowerPlane* have been estimated from real flight tests using a multi experiment Model-Based Parameter Estimation (MBPE) algorithm.

In this paper, we focus on the optimization of signal inputs that aim to maximize the information content of the measurement data used for determining the unknown model parameters. The paper is organized as follows. In Section II, the mathematical model of the *PowerPlane* for parameter estimation purposes is introduced and an overview of the flight test operation procedure and safety requirements is provided. Section III presents a formulation of the Optimum Experimental Design (OED) problem based on the Cramer-

Fig. 2. The second generation *PowerPlane* developed by Ampyx Power B.V. with mass $= 36.8$ kg, wing area $= 3$ m^2, wing span $= 5.5$ m and reference chord $= 0.55$ m.

This research was supported by the EU via ERC-HIGHWIND (259 166), ITN-TEMPO (607 957), ITN-AWESCO (642 682), by DFG via Research Unit FOR 2401, and by BMWi via the project eco4wind.

[1] Ampyx Power B.V, The Hague, 2521AL, The Netherlands
g.licitra@ampyxpower.com
p.williams@ampyxpower.com
r.ruiterkamp@ampyxpower.com

[2] Faculty of Management Science and Engineering, Karlsruhe University of Applied Sciences, 76133, Germany
adrian.buerger@hs-karlsruhe.de

[3] Department of Microsystems Engineering and Department of Mathematics, University of Freiburg, Germany 79110
moritz.diehl@imtek.uni-freiburg.de

Rao Lower Bound. The optimization problem is applied along the longitudinal axis of the *PowerPlane*. In Section IV, the performance of the optimized inputs is assessed for different degrees of inaccuracy of the a priori model. Finally, the optimized maneuvers are implemented in the Flight Control Computer (FCC) of the *PowerPlane* and validated using a high fidelity model and realistic atmospheric conditions.

II. MATHEMATICAL MODEL

In this section, the mathematical model of the *PowerPlane* is introduced, then a brief overview of the flight test procedures and safety requirements are provided.

A. Model Development

A rigid wing AWE pumping system can be modeled both via Differential Algebraic Equations (DAEs) [9][10][11] or by Ordinary Differential Equations (ODEs) [12]. For OED and Parameter Estimation (PE) purposes, let us consider the Flat-Earth, Body-Frame 6 Degree of Freedom equations of the *PowerPlane*

$$m \cdot \dot{\vec{v}}_b = \vec{F}_c + \vec{F}_p + \vec{F}_a + \vec{F}_g - m(\vec{\omega}_b \times \vec{v}_b) \tag{1a}$$

$$\mathrm{J} \cdot \dot{\vec{\omega}}_b = \vec{M}_c + \vec{M}_p + \vec{M}_a - (\vec{\omega}_b \times \mathrm{J} \cdot \vec{\omega}_b) \tag{1b}$$

$$\dot{\vec{\Phi}}_e = \mathrm{R} \cdot \vec{\omega}_b \tag{1c}$$

with (1a), (1b), (1c) the force, moment and kinematic equation of the aircraft with mass m and inertia J, respectively. The vectors $\vec{v}_b = [u, v, w]^T$ and $\vec{\omega}_b = [p, q, r]^T$ denote the translational and rotational speed vectors while $\dot{\vec{\Phi}}_e$ contains the rate of the Euler angles, i.e., of roll ϕ, pitch θ and yaw ψ which depend on the matrix R that is equal to

$$\mathrm{R} = \begin{bmatrix} 1 & \tan\theta\sin\phi & \tan\theta\cos\phi \\ 0 & \cos\phi & -\sin\phi \\ 0 & \frac{\sin\phi}{\cos\theta} & \frac{\cos\phi}{\cos\theta} \end{bmatrix}. \tag{2}$$

The aircraft is subject to forces $\vec{F}_*$ and moments $\vec{M}_*$ coming from the **c**able, **p**ropellers, **g**ravity and **a**erodynamics properties. Note that the gravity force vector $\vec{F}_g$ in Body-Frame is

$$\vec{F}_g = g \begin{bmatrix} -\sin\theta \\ \cos\theta\sin\phi \\ \cos\theta\cos\phi \end{bmatrix} \tag{3}$$

with $g \approx 9.81[\mathrm{m/s^2}]$.

Although the case study does not assume any propellers during power generation phase, they are present in the studied *PowerPlane* design for assisting launch and landing [13] as well as performing general purpose untethered flights. Finally, the mathematical model (1) is augmented with the so called *aerodynamic states* ,i.e., the airspeed V_T, angle of attack α and angle of side-slip β that for the no-wind case are as follows [14]

$$\dot{V}_T = \frac{u\dot{u} + v\dot{v} + w\dot{w}}{V_T} \tag{4a}$$

$$\dot{\alpha} = \frac{u\dot{w} - w\dot{u}}{u^2 + w^2} \tag{4b}$$

$$\dot{\beta} = \frac{\dot{v}V_T - v\dot{V}_T}{V_T\sqrt{u^2 + w^2}}. \tag{4c}$$

B. Flight Test Procedures and Safety Requirements

A flight test campaign aims to identify the aerodynamic properties of the aircraft, i.e., $\vec{F}_a$ and $\vec{M}_a$. In this case, $\vec{F}_a$ and $\vec{M}_a$ are defined as sums of terms which depend on the aircraft geometry, $\vec{\omega}_b$, α, β, V_T and control surfaces multiplied by coefficients known as *aerodynamic derivatives* (for details, see [8][15]).

Normally, it is rather difficult to have accurate models of the propellers and cable, hence the flight tests should be performed without cable such that $\vec{F}_c$ and $\vec{M}_c$ do not interfere with the overall aircraft dynamics. Additionally, propellers are switched off whenever an excitation signal occurs in order to decouple the thrust effects, simplifying (1a-1b) in

$$m \cdot \dot{\vec{v}}_b = \vec{F}_a + \vec{F}_g - m(\vec{\omega}_b \times \vec{v}_b) \tag{5a}$$

$$\mathrm{J} \cdot \dot{\vec{\omega}}_b = \vec{M}_a - (\vec{\omega}_b \times \mathrm{J} \cdot \vec{\omega}_b). \tag{5b}$$

Yet, system identification flight tests of piloted aircraft are carried out at a given trimmed airspeed. The excitation signal is performed by the pilot only along one axis in open-loop, while the other dynamics are kept under control.

The *PowerPlane* is an autonomous aircraft, hence no action of the pilot occurs during the flight test unless system failures are detected. As a consequence, reliable simulators play an important role for the design of maneuvers and minimization of flight envelope violation. Nonetheless, it may happen that during the real flight test the aircraft violates the flight envelope e.g. due to significant inaccuracies of the a priori models or unexpected gust that occurs during the open loop-phase. For this reason, *flight envelope limit detection* algorithms should be programmed in the FCC in order to avoid damages or complete destruction of the vehicle. Fig. 3 shows an example of how the flight envelope limit detection reacts right after the pitch angle θ violates its safety limit.

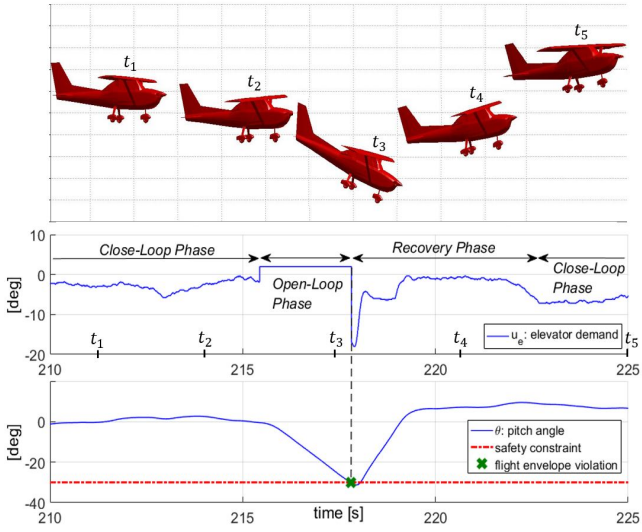

Fig. 3. Example of *flight envelope limit detection*. A badly designed maneuver is performed along the longitudinal axis via elevator deflection. The detection of flight envelope violation involves the stop of the open-loop phase, with recovery of the previous trim condition.

III. OPTIMUM EXPERIMENTAL DESIGN PROBLEM

In this section, an introduction of OED is given, then the a priori models and relative constraints for the longitudinal dynamics of the *PowerPlane* are provided.

A. Formulation of Optimum Experimental Design

The importance of choosing appropriate control inputs for extraction of the *aerodynamic derivatives* from flight test data was first noted by Gerlach [16]. Subsequent research focused on design techniques for optimal control input signals that aim to [17]

- maximize the information content of the flight test data;
- minimize the length of flight test maneuver necessary to reach a specified level of accuracy of the *aerodynamic derivatives*;
- reduce the number of expensive system identification flight tests.

The main idea of OED is to use an operator norm $\Psi(.)$ of the Fisher information matrix M as a criterion of an optimization problem. The inverse of the Fisher information matrix yields a universal lower bound on parameter estimation accuracies known as the Cramer-Rao Lower Bound, which allows to optimize the input signal regardless the type of estimation algorithm implemented [18].

In this context, let us consider a mathematical model known a priori and defined as a set of ODEs

$$\dot{\mathbf{x}}(t) = \mathbf{f}(\mathbf{x}(t), \mathbf{u}(t), \theta_p), \;\; \mathbf{x}(0) = \mathbf{x}_0, \;\; t \in [0, T] \tag{6a}$$

$$\mathbf{y}(t) = \mathbf{h}(\mathbf{x}(t), \mathbf{u}(t), \theta_p) \tag{6b}$$

$$\mathbf{y}_m(i) = \mathbf{y}(i) + \varepsilon(i), \qquad i = 1, ..., N \tag{6c}$$

with differential states $\mathbf{x} \in \mathbb{R}^{n_x}$, output states $\mathbf{y} \in \mathbb{R}^{n_y}$, control inputs $\mathbf{u} \in \mathbb{R}^{n_u}$, a priori parameters $\theta_p \in \mathbb{R}^{n_\theta}$. The output $\mathbf{y}_m$ is sampled in N measurements along a time horizon T and it is polluted by additive, zero-mean Gaussian noise $\varepsilon \approx \eta(0, \Sigma_y)$ with $\Sigma_y \in \mathbb{R}^{n_y \times n_y}$ the measurements noise covariance matrix. In agreement with the notation in (6), the Fisher information matrix can be expressed as

$$\mathrm{M} = \sum_{i=1}^{N} \left[\left(\frac{\partial \mathbf{y}(i)}{\partial \theta_p} \right)^T \Sigma_y^{-1} \left(\frac{\partial \mathbf{y}(i)}{\partial \theta_p} \right) \right]. \tag{7}$$

Therefore, a general model-based OED problem which considers input and output constraints can be formulated in the form

$$\underset{\mathbf{x}(\cdot), \mathbf{u}(\cdot)}{\text{minimize}} \qquad \Psi(\mathrm{M}[\mathbf{x}(\cdot), \mathbf{u}(\cdot), \theta_p]) \tag{8a}$$

$$\text{subject to:} \qquad \dot{\mathbf{x}}(t) = \mathbf{f}(\mathbf{x}(t), \mathbf{u}(t), \theta_p), \;\; t \in [0, T] \tag{8b}$$

$$\mathbf{x}(0) = \mathbf{x}_0, \tag{8c}$$

$$\mathbf{u}_{\min} \leq \mathbf{u}(t) \leq \mathbf{u}_{\max}, \qquad t \in [0, T] \tag{8d}$$

$$\mathbf{x}_{\min} \leq \mathbf{x}(t) \leq \mathbf{x}_{\max}. \qquad t \in [0, T] \tag{8e}$$

Different operator norms can be used in (8) with different features [19][20][21]. In this paper, we use the so called *A-criterion* [22] that consider as objective function

$$\Psi(\mathrm{M}) = \frac{1}{n_\theta} \cdot \mathrm{trace}\left(\mathrm{M}^{-1}\right) = \frac{1}{n_\theta} \cdot \mathrm{trace}\left(\Sigma_\theta\right) \tag{9}$$

with Σ_θ the parameter covariance matrix. In other words the *A-criterion* minimizes the sums of the variances of the estimated parameters relative to the a priori ones. In the next section, the OED theory is applied to the longitudinal dynamics of the *PowerPlane*.

B. A Priori Model

For aircraft PE experiments, typically a linear perturbation model structure is assumed. As a consequence, the flight test inputs are perturbations about a trim condition so that the system response can be adequately modeled by such linear structure [23]. For small side-slip angle β it is possible to decouple the aircraft dynamics in longitudinal and lateral dynamics [14]. Let us consider the longitudinal dynamics only, hence the Linear Time-Invariant (LTI) system of the *PowerPlane* will be

$$\dot{\mathbf{x}}_{\text{long}} = A\,\mathbf{x}_{\text{long}} + B\,\mathbf{u}_{\text{long}} \tag{10}$$

with $\mathbf{x}_{\text{long}} = \begin{bmatrix} V_T & \alpha & \theta & q \end{bmatrix}^T$ and $\mathbf{u}_{\text{long}} = \delta_e$ where δ_e denotes the elevator deflection while the state and input matrix are

$$A = \begin{bmatrix} P_{v_T} & P_\alpha & g\cos(\gamma) & P_q \\ S_{v_T} & S_\alpha & 0 & S_q \\ 0 & 0 & 0 & 1 \\ M_{v_T} & M_\alpha & 0 & M_q \end{bmatrix}, \tag{11a}$$

$$B = \begin{bmatrix} P_{\delta_e} & S_{\delta_e} & 0 & M_{\delta_e} \end{bmatrix}^T. \tag{11b}$$

The coefficients P_*, S_*, M_* denote the *dimensional aerodynamic derivatives* which shall be identified by the system identification flight test. Note that the *aerodynamic derivatives* vary for different trim conditions. The quantity $g\cos(\gamma)$ is assumed to be known and comes from the linearization point where γ refers to flight path angle. Finally, in order to take into account the rate of elevator deflection, the system is augmented as follows:

$$\dot{\tilde{\mathbf{x}}} = A_{\text{aug}}\,\tilde{\mathbf{x}} + B_{\text{aug}}\,\tilde{\mathbf{u}} \tag{12a}$$

$$A_{\text{aug}} = \begin{bmatrix} A & B \\ 0_{1\times 4} & 0 \end{bmatrix} \tag{12b}$$

$$B_{\text{aug}} = \begin{bmatrix} 0 & 0 & 0 & 0 & 1 \end{bmatrix}^T \tag{12c}$$

with $\tilde{\mathbf{x}} = \begin{bmatrix} \mathbf{x}_{\text{long}} & \mathbf{u}_{\text{long}} \end{bmatrix}^T$ and $\tilde{\mathbf{u}} = \dot{\mathbf{u}}_{\text{long}}$. The optimization problem (8) will be subject to the a priori model (12a). The a priori *aerodynamic derivative* θ_p can be provided by CFD, lifting line, previous flight tests or a combination of those. In this paper, we considered a trim condition for $V_T = 20\,[\mathrm{m/s}]$, and flap setting $\delta_f = 0\,[\mathrm{deg}]$ where $g\cos(\gamma) = -9.8066$. The measurement noise standard deviation used for Σ_y are shown in Table I while the assumed "true" *dimensional aerodynamic derivatives* are in Table II.

C. Constraints

In general, hard constraint are not very relevant in input signal design for flight tests unless a flight test maneuver is planned at the edge of the permissible flight envelope [17]. For this case study, the constraints have been chosen as follows

- elevator deflection δ_e, angle of attack α as well as the airspeed V_T were constrained in order to keep the aircraft within the region where the linear model is applicable;
- rate of elevator deflection $\dot{\delta}_e$ was constrained according to the maximum speed of the installed servos;
- pitch rate q and pitch angle θ should be bounded with respect to the flight envelope limits since any violation of the flight envelope would result in abortion of the system identification test. In order to take into account model mismatch and inaccuracies of the a priori *aerodynamic derivatives*, these bounds were enforced with a safety margin.

In Table III, input and state constraints are summarized.

D. Initial Input Signal

The optimization problem (8) needs to be initialized with a suitable input signal. The initial maneuver chosen for this application is widely used in the aerospace field due to its easy implementation and good estimation performance [17]. In turn, such input signal comes from an optimization procedure of a sequence of step functions, developed by Koehler [24]. The aim of Koehler was to find a signal with a shape as simple as possible and power distributed uniformly over a wide range of frequencies [25]. The input signal had a *bang-bang* behavior with a duration $7\Delta T$ where the switching times were at $t = 3\Delta T$, $t = 5\Delta T$, and $t = 6\Delta T$. For this reason, such an input signal was called a *3-2-1-1 maneuver*. Fig. 4 shows a *3-2-1-1 maneuver* of amplitude $A = 5[\text{deg}]$ subject to limited rate deflection in agreement with the *PowerPlane* servos.

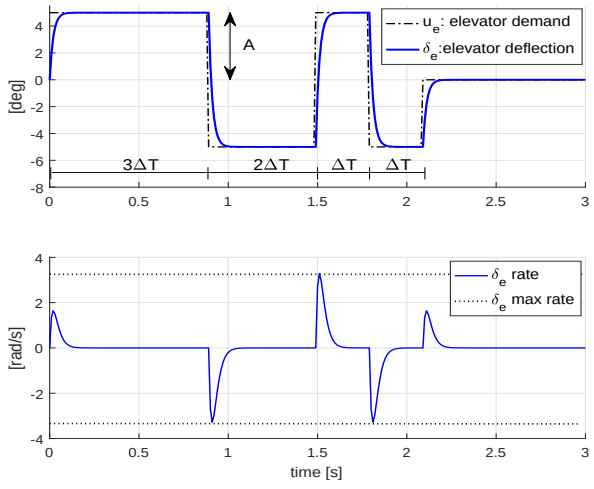

Fig. 4. Example of a *3-2-1-1 maneuver* subject to limited speed.

E. Algorithm Implementation

The optimization problem (8) requires frequent evaluation of the parameter covariance matrix Σ_θ, hence an efficient evaluation of this matrix is crucial from a computational point of view [26],[27]. In this paper, the optimized maneuvers are obtained using the open-source Python module CASIOPEIA [28] based on CasADi [29] with IPOPT as NLP solver [30]. CASIOPEIA computes the covariance matrix Σ_θ from the inverse of the KKT-matrix of the underlying parameter estimation problem using a Schur Complement approach which relies on the solution of a sparse linear system and the inversion of a small-scale matrix with dimension equal to the number of estimated parameters. The method and implementation details are shown in [31]. The continuous-time optimization problem is discretized and formulated as a nonlinear program automatically via direct collocation [32] using Lagrange polynomials.

IV. ANALYSIS & RESULTS

In order to assess the performance of the optimized maneuvers, three hypothetical cases are taken into account:

- a case during the preliminary phase of the flight test campaign where *aerodynamic derivatives* come exclusively from simulation, hence high inaccuracies might be present;
- a case during an intermediate stage of the flight test campaign where *aerodynamic derivatives* rely on both simulation and previous flight tests, hence reasonable estimates are expected;
- a case after an extensive flight test campaign where *aerodynamic derivatives* are likely to have high accuracy.

We assume that the a priori parameters θ_p deviate in percentage w.r.t. the "true" parameter θ_0 by $\Delta\theta_{\%} = 100\%$, $\Delta\theta_{\%} = 20\%$ and $\Delta\theta_{\%} = 5\%$, respectively. For each case, *3-2-1-1 maneuvers* were designed to both provide good Signal-Noise-Ratio (SNR) and keep the system response within the prescribed constraints in agreement with the a priori models. Such design was carried out via qualitative considerations in the frequency domain, too [17]. For comparability, the maneuvers were injected into the "true model" in order to verify the impact of the *3-2-1-1 maneuvers* based on inaccurate models (see Fig. 5). In all cases, the duration of the maneuvers was set to $T = 10[\text{s}]$.

Afterwards, the a priori *aerodynamic derivatives* and *3-2-1-1 maneuvers* were used to initialize the optimization problem (8) subject to the model (12). Fig. 6 and Fig. 7 show the optimized inputs and optimized responses, respectively.

One can observe that in all three cases, the optimized maneuvers have a *bang-bang* behavior where the transition values occur with a slope which corresponds to the speed of the installed servos. However, the rate of elevator deflection does not exploit its maximum allowable limit (see fourth graph of Fig. 6). The angle of attack α, pitch angle θ and pitch rate q approach to a sinusoidal response while the airspeed V_T increases in agreement with the prescribed constraints. As for the *3-2-1-1 maneuvers*, the optimized maneuvers were performed considering no model mismatch. The results show that even for the worst case ($\Delta\theta_{\%} = 100\%$) there is no significant constraints violation.

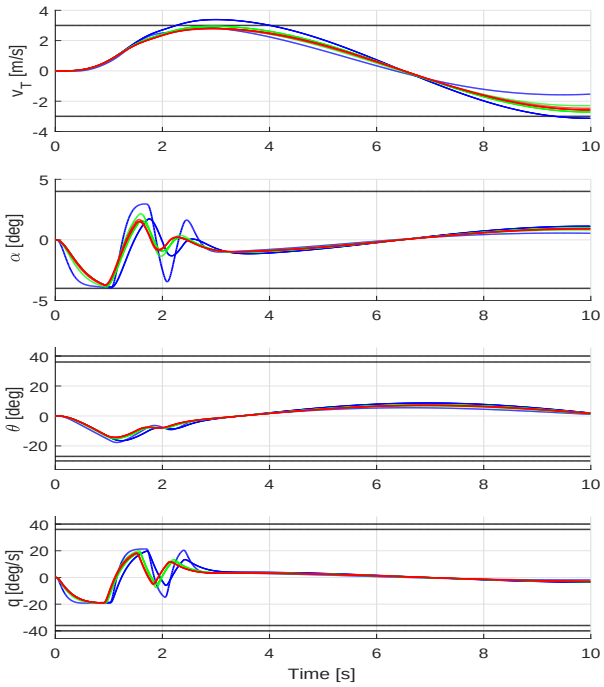

Fig. 5. Output response using *3-2-1-1 maneuvers*. The a priori model responses are in dash-dot line while the true model responses are in solid line. The output responses blue line for the case $\Delta\theta_{\%} = 100\%$, green line for the case $\Delta\theta_{\%} = 20\%$, red line for the case $\Delta\theta_{\%} = 5\%$. Flight envelope limits in black dash-dot line while the constraints are in black dot line.

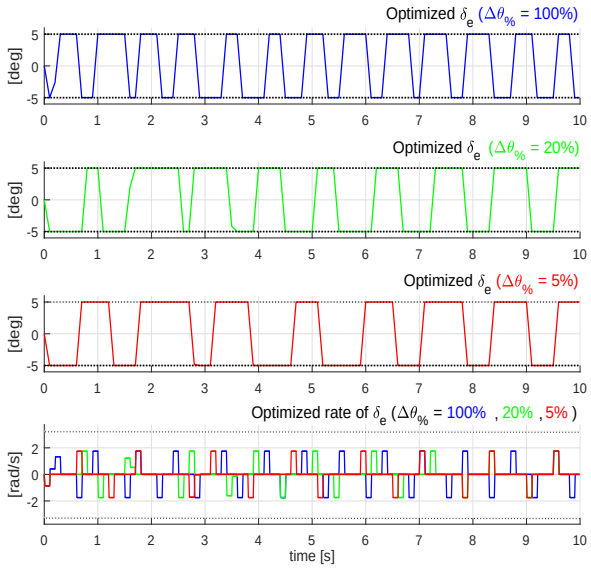

Fig. 6. Optimized maneuvers with respective rate of inputs for the case $\Delta\theta_{\%} = 100\%$ (blue line), $\Delta\theta_{\%} = 20\%$ (green line),$\Delta\theta_{\%} = 5\%$ (red line). Dot lines refer to constraints.

A. Assessment of Estimation Performance

Estimation performance for the data obtained by both *3-2-1-1 maneuvers* and optimized maneuvers were assessed via a Maximum Likelihood approach [33] where 1-σ confidence ellipsoids were computed [8] via an estimate of the covariance matrix Σ_θ [34] using 1000 experiments. Due to space limitation, only the 1-σ confidence ellipsoids for the pair of estimates (P_{δ_e}, P_q), (S_{δ_e}, P_α), (M_q, M_α) are shown in Fig. 8, 9. Note that, $P_{v_T}, P_\alpha, P_q, P_{\delta_e}$ belong to the *phugoid mode* [14] and their estimation with reasonable accuracy is rather difficult via elevator deflection.

Table IV shows the deviation of the variance in percentage between the initial and optimized maneuvers. A negative value means a reduction of the variance, in other words an improvement in terms of estimation accuracy and vice versa for positive values. One can observe that the optimized maneuvers provide a better estimation accuracy in comparison to the *3-2-1-1 maneuvers*. More reliable a priori models facilitate higher information content of the optimized experiment. However, for high parameter inaccuracies a loss of estimation performance for the *aerodynamic derivatives* relative to the airspeed dynamics has been shown.

B. Simulation with realistic atmospheric condition

Once the maneuvers performances have been validated, a flight plan must be set. As mentioned before, the *PowerPlane* is an autonomous aircraft, hence it has to launch, perform the system identification flight test and land safely without any action from the pilot (in remote). The FCC of the case study allows to define maneuvers as steps with tunable amplitude and time length only. Therefore, the steps transition shown in Fig. 6 were approximated as tight step functions. The results obtained from the high fidelity simulator designed by Ampyx Power B.V. show that the *PowerPlane* was able to complete the system identification flight test without any flight envelope violation, providing good excitation of the longitudinal dynamics, see Fig. 10,12,11,13.

V. CONCLUSIONS

In this paper, a model-based optimum experimental design has been applied to a rigid wing AWE pumping system. The optimized maneuvers were obtained for a trim condition of the aircraft longitudinal dynamics and implemented in the *PowerPlane* Flight Computer Control. The optimization problem was initialized using a priori *aerodynamic derivatives* for different (hypothetical) stages of a flight test campaign and using the well known and widely used *3-2-1-1 maneuvers*. The results have shown that with reasonable a priori models, optimized maneuvers can improve the information content of the experiment data significantly. However, it is advisable to apply conventional signal inputs like the *3-2-1-1 maneuver* during the preliminary stage of the flight test campaign.

VI. FUTURE WORKS

Future works will aim towards the validation of the optimized maneuvers with real system identification flight tests.

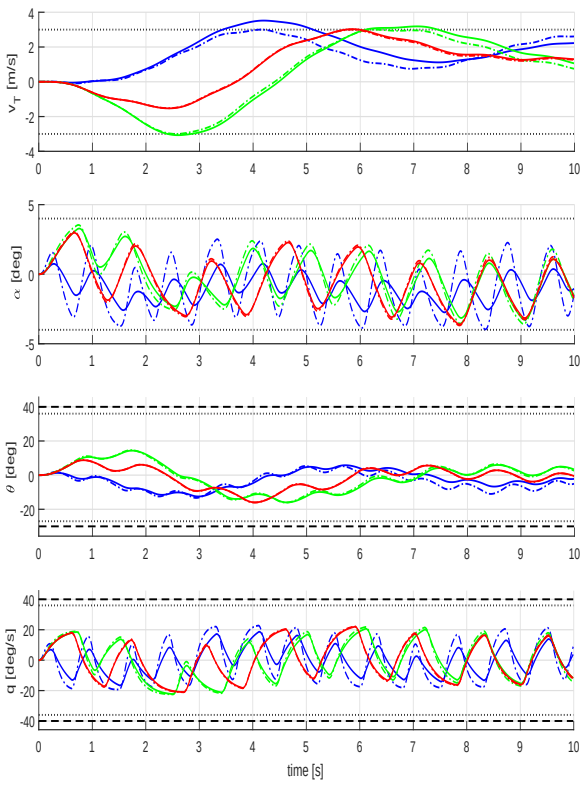

Fig. 7. Output response using optimized maneuvers. The a priori model responses are in dash-dot line while the true model responses are in solid line. The output responses are in blue line for the case $\Delta\theta_{\%} = 100\%$, green line for the case $\Delta\theta_{\%} = 20\%$, red line for the case $\Delta\theta_{\%} = 5\%$. Flight envelope limits in black dash-dot line while the constraints are in black dot line.

TABLE I

SENSORS NOISE STANDARD DEVIATION σ

Variable	σ	Unit
v_T	0.4	[m/s]
α	0.0175 (0.1)	[rad] (deg)
θ	0.0349 (0.2)	[rad] (deg)
q	0.0175 (0.1)	[rad/s] (deg/s)

TABLE II

TRUE DIMENSIONAL AERODYNAMIC DERIVATIVES

Parameters	θ_0
P_{v_T}	-0.0688
P_α	+6.2603
P_q	-0.1606
P_{δ_e}	-0.1819
S_{v_T}	-0.0491
S_α	-4.9292
S_q	+0.8962
S_{δ_e}	-0.3148
M_{v_T}	-0.0068
M_α	-7.6875
M_q	-1.9631
M_{δ_e}	-13.1733

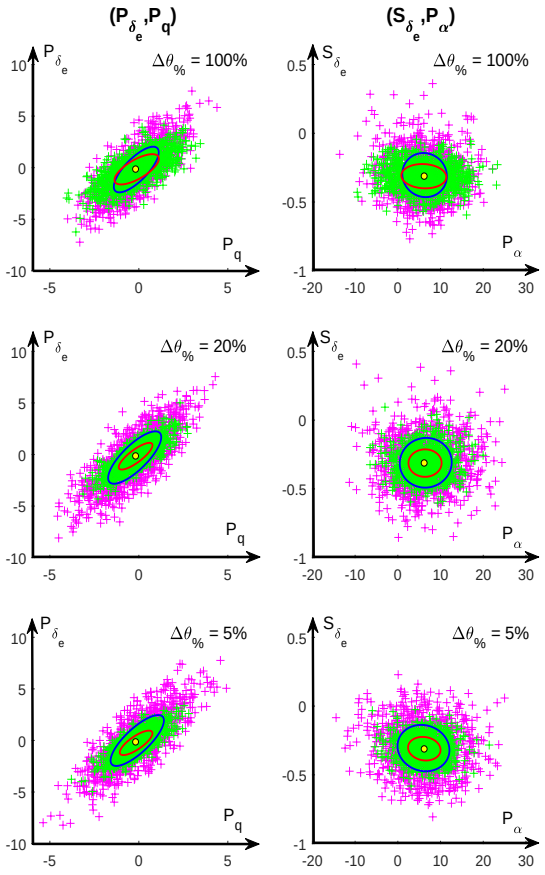

Fig. 8. 1-σ confidence ellipsoids for the pair of estimates (P_{δ_e}, P_q) (left column) and (S_{δ_e}, P_α) (right column). 1000 experiments have been performed for the cases $\Delta\theta = 100\%$, $\Delta\theta = 20\%$, $\Delta\theta = 5\%$. The true parameters are denoted with yellow circle marker. The cross markers refers the estimate of the parameters using initial maneuvers (+ marker) and optimized maneuvers (+ marker). Confidence ellipsoids are in blue line initial experiments and in(red line) for the optimized experiments.

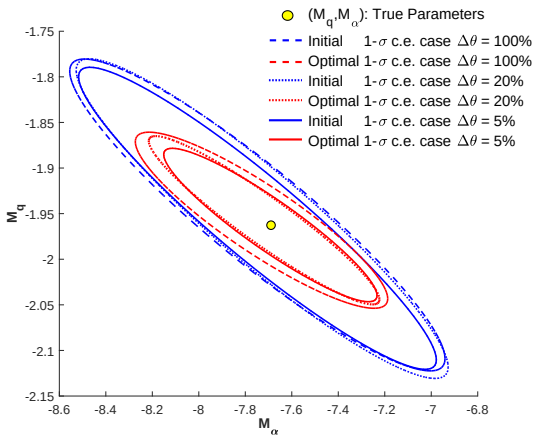

Fig. 9. Comparison between initial and optimal 1-σ confidence ellipsoids (c.e.) for the pair of estimates (M_q, M_α) for the cases $\Delta\theta = 100\%, 20\%, 5\%$. In all cases, the optimized maneuvers provide better estimation accuracy w.r.t. *3-2-1-1 maneuvers*.

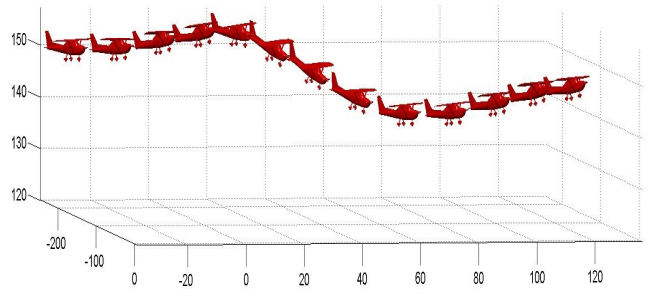

Fig. 10. Aircraft behavior during the system identification flight test.

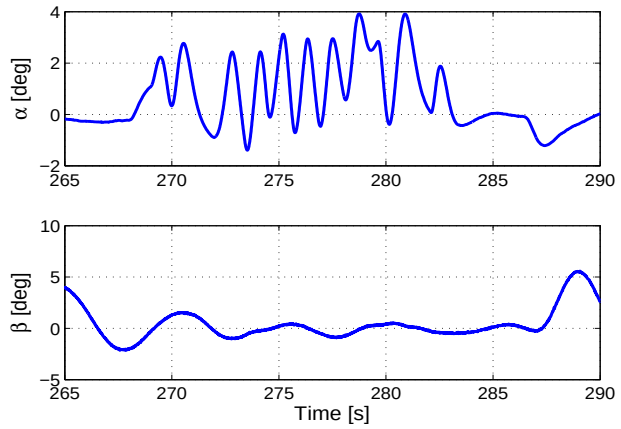

Fig. 11. Angle of attack α and angle of side slip β related to Fig. 10. For small angle of side slip, the aircraft dynamic can be decoupled in longitudinal and lateral dynamics.

TABLE III

INPUT AND STATE CONSTRAINTS

Constraints	Values	Unit
$\delta_{e_{\min}}$, $\delta_{e_{\max}}$	$-5,5$	[deg]
$\dot{\delta}_{e_{\min}}$, $\dot{\delta}_{e_{\max}}$	$-3.25,3.25$	[rad/s]
$\alpha_{\min}$, $\alpha_{\max}$	$-4,4$	[deg]
$V_{\min}$, $V_{\max}$	$-3,3$	[m/s]
$q_{\min}$, $q_{\max}$	$-36,36$	[deg]
$\theta_{\min}$, $\theta_{\max}$	$-27,36$	[deg/s]

TABLE IV

VARIANCE REDUCTION IN PERCENTAGE

$\Delta\sigma^2_{\%}$ derivatives	$\Delta\theta_{\%}$ 100%	20%	5%
P_{v_T}	+5.85%	-59.24%	-61.22%
P_α	+1.75%	-59.33%	-60.81%
P_q	-2.21%	-59.62%	-62.50%
P_{δ_e}	-56.0%	-73.92%	-76.94%
S_{v_T}	-39.47%	-63.98%	-68.58%
S_α	-41.13%	-62.01%	-62.84%
S_q	-53.82%	-69.96%	-70.20%
S_{δ_e}	-69.63%	-69.48%	-74.17%
M_{v_T}	-49.13%	-65.36%	-74.14%
M_α	-50.21%	-61.52%	-67.71%
M_q	-66.0%	-72.24%	-75.81%
M_{δ_e}	-78.29%	-69.61%	-77.59%

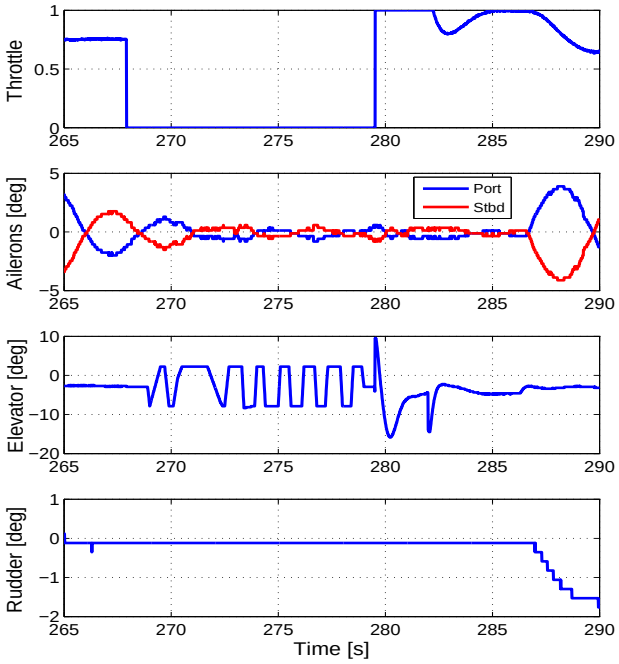

Fig. 12. Control demands related to Fig. 10. The optimal maneuver (case $\Delta\theta = 20\%$) was performed along the longitudinal axis by elevator deflection while the lateral dynamics were stabilized by aileron and rudder deflection.

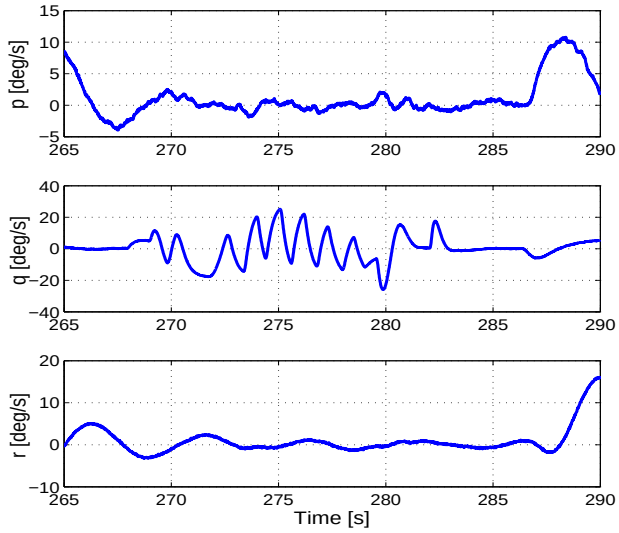

Fig. 13. Roll p, pitch q and yaw r rate related to Fig. 10. The pitch rate q is the only body rate excited due to the decoupling effect.

APPENDIX

REFERENCES

[1] M. L. Loyd, "Crosswind kite power (for large-scale wind power production)," *Journal of energy*, vol. 4, no. 3, pp. 106–111, 1980.

[2] M. Diehl, R. Schmehl, and U. Ahrens, *Airborne Wind Energy. Green Energy and Technology*. Springer Berlin Heidelberg, 2014.

[3] M. Diehl, "Airborne wind energy: Basic concepts and physical foundations," in *Airborne Wind Energy*. Springer, 2013, pp. 3–22.

[4] L. Fagiano and M. Milanese, "Airborne wind energy: an overview," in *American Control Conference (ACC), 2012*. IEEE, 2012, pp. 3132–3143.

[5] AP. (2016) Ampyx power: Airborne wind energy. [Online]. Available: https://www.ampyxpower.com/

[6] H. K. Versteeg and W. Malalasekera, *An introduction to computational fluid dynamics: the finite volume method*. Pearson Education, 2007.

[7] J. D. Anderson Jr, *Fundamentals of aerodynamics*. Tata McGraw-Hill Education, 2010.

[8] G. Licitra, P. Williams, J. Gillis, S. Ghandchi, S. Sieberling, R. Ruiterkamp, and M. Diehl, "Aerodynamic parameter identification for an airborne wind energy pumping system," in *IFAC 2017 World Congress, Toulouse, France. 9-14 July*, 2017.

[9] S. Gros and M. Diehl, "Modeling of airborne wind energy systems in natural coordinates," in *Airborne wind energy*. Springer, 2013, pp. 181–203.

[10] P. Williams, B. Lansdorp, and W. Ockels, "Modeling and control of a kite on a variable length flexible inelastic tether," in *AIAA Guidance, navigation and control conference*, 2007.

[11] P. Williams, B. Lansdorp, R. Ruiterkamp, and W. Ockels, *Modeling, simulation, and testing of surf kites for power generation*. American Institute of Aeronautics and Astronautics, 2008.

[12] R. Ruiterkamp and S. Sieberling, "Description and preliminary test results of a six degrees of freedom rigid wing pumping system," in *Airborne wind energy*. Springer, 2013, pp. 443–458.

[13] J. Koenemann, P. Williams, S. Sieberling, and M. Diehl, "Modeling of an airborne wind energy system with a flexible tether model for the optimization of landing trajectories," in *IFAC 2017 World Congress, Toulouse, France. 9-14 July*, 2017.

[14] B. L. Stevens, F. L. Lewis, and E. N. Johnson, *Aircraft Control and Simulation: Dynamics, Controls Design, and Autonomous Systems*. John Wiley & Sons, 2015.

[15] J. Mulder, W. Van Staveren, and J. van der Vaart, *Flight dynamics (lecture notes): ae3-302*. TU Delft, 2000.

[16] O. H. Gerlach, "Analyse van een mogelijke methode voor het meten van prestaties en stabiliteits-en besturingseigenschappen van een vliegtuig in niet-stationaire, symmetrische vluchten (analysis of a possible method for the measurement of performance and stability and control characteristics in non-steady symmetrical flight)," *Technische Hogeschool Delft, Vliegtuigbouwkunde, Rapport VTH-117*, 1964.

[17] J. Mulder, J. Sridhar, and J. Breeman, "Identification of dynamic system-application to aircraft nonlinear analysis and manoeuvre design," Technical Report AG 300, AGARD, Tech. Rep., 1994.

[18] E. A. Morelli, *Practical input optimization for aircraft parameter estimation experiments*. National Aeronautics and Space Administration, Langley Research Center, 1993.

[19] N. K. Gupta and W. E. Hall Jr, "Input design for identification of aircraft stability and control derivatives," 1975.

[20] N. Nahi and D. Wallis, "Optimal inputs for parameter estimation in dynamic systems with white observation noise," in *Joint Automatic Control Conference*, no. 7, 1969, pp. 506–513.

[21] N. Nahi and G. Napjus, "Design of optimal probing signals for vector parameter estimation," in *Decision and Control, 1971 IEEE Conference on*, vol. 10. IEEE, 1971, pp. 162–168.

[22] R. K. Mehra and N. Eupta, "Status of input design for aircraft parameter identification," 1975.

[23] V. Klein, "Optimal input design for aircraft parameter estimation using dynamicprogramming principles," in *17th Atmospheric Flight Mechanics Conference*, 1990, p. 2801.

[24] R. Koehler and K. Wilhelm, "Auslegung von eingangssignalen für die kennwertermittlung," *DFVLR-IB*, pp. 154–77, 1977.

[25] E. Plaetschke and G. Schulz, "Practical input signal design," *AGARD Lecture Series*, vol. 104, 1979.

[26] S. Körkel, "Numerische Methoden für optimale Versuchsplanungsprobleme bei nichtlinearen DAE-Modellen," Ph.D. dissertation, 2002.

[27] E. Kostina and O. Kostyukova, "Computing covariance matrices for constrained nonlinear large scale parameter estimation problems using krylov subspace methods," in *Constrained Optimization and Optimal Control for Partial Differential Equations*. Springer, 2012, pp. 197–212.

[28] A. Bürger. (2016) Casiopeia: Casadi interface for optimum experimental design and parameter estimation and identification applications. [Online]. Available: https://github.com/adbuerger/casiopeia

[29] J. Andersson, "A General-Purpose Software Framework for Dynamic Optimization," PhD thesis, Arenberg Doctoral School, KU Leuven, Department of Electrical Engineering (ESAT/SCD) and Optimization in Engineering Center, Kasteelpark Arenberg 10, 3001-Heverlee, Belgium, October 2013.

[30] A. Wächter and L. T. Biegler, "On the implementation of an interior-point filter line-search algorithm for large-scale nonlinear programming," *Mathematical programming*, vol. 106, no. 1, pp. 25–57, 2006.

[31] A. Bürger, D. Kouzoupis, A. Altmann-Dieses, and M. Diehl, "A schur complement method for optimum experimental design in the presence of process noise." Proceedings of the IFAC world congress, 2007.

[32] L. T. Biegler, *Nonlinear programming: concepts, algorithms, and applications to chemical processes*. SIAM, 2010.

[33] L. Ljung, "System identification: Theory for the user." Prentice Hall PTR, 1998.

[34] H. G. Bock, T. Carraro, W. Jäger, S. Körkel, R. Rannacher, and J. Schlöder, *Model Based Parameter Estimation: Theory and Applications*. Springer Science & Business Media, 2013, vol. 4.